



Published in final edited form as:

Med Image Anal. 2015 January ; 19(1): 164–175. doi:10.1016/j.media.2014.09.006.

Sequential Monte Carlo Tracking of the Marginal Artery by Multiple Cue Fusion and Random Forest Regression

Kevin M. Cherry, Brandon Peplinski, Lauren Kim, Shijun Wang, Le Lu, Weidong Zhang, Jianfei Liu, Zhuoshi Wei, and Ronald M. Summers

Imaging Biomarkers and Computer-Aided Diagnosis Laboratory, Radiology and Imaging Sciences, National Institutes of Health Clinical Center, Building 10 Room 1C224D MSC 1182 Bethesda, MD 20892-1182

Abstract

Given the potential importance of marginal artery localization in automated registration in computed tomography colonography (CTC), we have devised a semi-automated method of marginal vessel detection employing sequential Monte Carlo tracking (also known as particle filtering tracking) by multiple cue fusion based on intensity, vesselness, organ detection, and minimum spanning tree information for poorly enhanced vessel segments. We then employed a random forest algorithm for intelligent cue fusion and decision making which achieved high sensitivity and robustness. After applying a vessel pruning procedure to the tracking results, we achieved statistically significantly improved precision compared to a baseline Hessian detection method (2.7% versus 75.2%, $p < 0.001$). This method also showed statistically significantly improved recall rate compared to a 2-cue baseline method using fewer vessel cues (30.7% versus 67.7%, $p < 0.001$). These results demonstrate that marginal artery localization on CTC is feasible by combining a discriminative classifier (i.e., random forest) with a sequential Monte Carlo tracking mechanism. In so doing, we present the effective application of an anatomical probability map to vessel pruning as well as a supplementary spatial coordinate system for colonic segmentation and registration when this task has been confounded by colon lumen collapse.

Keywords

sequential Monte Carlo tracking; multiple cue fusion; particle filtering; random forest; computer-aided detection; marginal artery; CT angiography

*Corresponding author and reprint requests: Ronald M. Summers, M.D., Ph.D., Senior Investigator and Staff Radiologist, Imaging Biomarkers and Computer-Aided Diagnosis Laboratory Radiology and Imaging Sciences, National Institutes of Health Clinical Center, Building 10 Room 1C224D MSC 1182, Bethesda, MD 20892-1182, Phone: (301) 402-5486, Fax: (301) 451-5721 rms@nih.gov http://www.cc.nih.gov/about/SeniorStaff/ronald_summers.html.

Publisher's Disclaimer: This is a PDF file of an unedited manuscript that has been accepted for publication. As a service to our customers we are providing this early version of the manuscript. The manuscript will undergo copyediting, typesetting, and review of the resulting proof before it is published in its final citable form. Please note that during the production process errors may be discovered which could affect the content, and all legal disclaimers that apply to the journal pertain.

Presented in part at the 16th International Conference on Medical Image Computing and Computer Assisted Intervention, 2013.

1. Introduction

Colorectal cancer is the second leading cause of cancer-related death in the United States with over 50,000 deaths reported per annum (Siegel et al., 2013). Key to the reduction in mortality rate is early detection of colorectal polyps. Computed tomography colonography (CTC) is an accurate and safe method of colon cancer screening, and computer-aided diagnosis (CAD) systems implemented in tandem potentially improve a radiologist's detection performance (Dachman et al., 2010; Halligan et al., 2011; Johnson et al., 2008; Pickhardt et al., 2003; Summers et al., 2005). A standard CTC protocol requires patients to be scanned in both supine and prone position, thereby reducing false positive polyp detections and significantly improving sensitivity (Chen et al., 1999; Yee et al., 2003). Registration of supine-prone images relies upon either brute-force mental visualization by the interpreting radiologist or automated methods based on anatomic landmarks such as the hepatic and splenic flexures, haustral folds, or prominent longitudinal bands of smooth muscle known as the teniae coli (Hampshire et al., 2011; Roth et al., 2011; Wang et al., 2011). Unfortunately, both mental visualization and automated registration based on these aforementioned anatomic landmarks can be confounded by lumen collapse. To address this problem, Wei et al. (2013) have recently proposed the use of the marginal artery (MA) and vein as a supplementary axis to coordinate supine-prone image registration. The marginal artery and vein, which courses along the longitudinal axis of the colon parallel to its mesenteric attachment, lie extrinsic to the colon and are therefore generally unaffected by lumen collapse (Fig. 1). Here we present a semi-automated method of detecting the marginal vessels on CT angiography (CTA) using sequential Monte Carlo (SMC) tracking so that a spatial coordinate system fiducial marker extrinsic to the colon may be attained.

2. Background

Vessel enhancement filtering, region growing, active contours, centerline extraction, and stochastic framework are five major approaches to 3D vessel detection and segmentation (Lesage et al., 2009). Among these methods, sequential Monte Carlo tracking, also known as particle filtering, is a stochastic solution that has been widely used in various tracking problems due to its accuracy, robustness, and computational feasibility. Frangi et al. (1998) first proposed a vessel enhancement filtering algorithm based on local multi-scale second order Hessian structure analysis of an image. The benefit of this technique was demonstrated on aortoiliac and cerebral magnetic resonance angiograms (MRA). While filtering enhancement-based methods (e.g. Frangi and Li's vesselness detectors) demonstrate high sensitivity, they also have a high false positive rate for MA segmentation. Region growing based methods are easy to implement and usually work well on large vessels such as the aorta. However, they demonstrate poorer performance in the detection of small or poorly enhanced vessels like the MA. Additionally, region growing-based methods commonly demonstrate leakage into large organs which further exacerbates its false positive rate. Active contour-based methods are very effective on large vessels on 2D images, but perform less well on smaller, higher order vessels such as the MA due to its small caliber and complex branching pattern, corroborating the inherent difficulty in designing a universal internal, model-based force and external force for segmentation surface evolution.

Many investigators have contributed to the stochastic-based vessel tracking field in recent years. Florin et al. (2005) proposed a particle filtering-based approach for the detection of coronary arteries. In their model, state variables included position, orientation, shape, and vessel appearance. Later, Schaap *et al.* (2007) presented a Bayesian tracking framework for tubular structures such as carotid arteries in CTA. The key contribution of their work was a novel observation model designed for tube-like objects which consisted of a series of tube segments identified by location, orientation, radius, intensity, and intensity variance. Lacoste et al. (2006) employed Markov marked point processes for the detection of coronary arteries on 2D CTA. Multiple investigators have used SMC- based vessel segmentation methods (Florin et al., 2005; Lacoste et al., 2006; Schaap et al., 2007) to fit the probabilistic model and make it computationally feasible, an approach which worked with large vessels. However, this approach is less successful with MA tracking and segmentation due to insufficient information employed for tracking. More recently, Friman et al. (2010) proposed a multiple hypothesis template tracking scheme for small 3D vessel structures. For other advances in the field of vessel detection and segmentation, readers may wish to refer to the recent review paper on this topic (Lesage et al., 2009).

SMC has also been used in computer vision to handle problems such as athlete or vehicle tracking in video sequences (Kristan et al., 2009; Zhou et al., 2004). For tracking, the collection and utilization of more target and background information typically provide increased accuracy and robustness for a given noise level. In recent years, incorporating multiple cues in the Bayesian tracking framework has been a focus of research for multiple investigators. Wu and Huang (2004) proposed a factorized graphical model to integrate multiple cues for Bayesian tracking. The authors asserted that the inference of a high-dimensional state space could be factorized into many lower-dimensional state spaces to discover their co-inference. The main idea was that the use of several cues with rough models would be more robust and computationally efficient than a complex single cue model. Brasnett et al. (2007) proposed visual cues including color, edge, and texture for object tracking in video sequences. This work also included a multi-component, mixed dynamic model for motion prediction and a robust way to deal with target occlusion. Visual cues were histogram based, weighted adaptively, and represented in likelihood functions employing the Bhattacharyya distance. The work of Moreno-Noguer et al. (2008) focused on integrating multiple dependent cues for robust tracking. Cue dependence was considered and each feature was represented by a separate Bayesian filter. The group used object bounding box, Fisher color space, target and background color distributions, and object contour in a hypothesis-generation, hypothesis-correction format to create a generalized, probabilistic framework. Spengler and Schiele (2003) demonstrated the robustness of an adaptively weighted multi-cue fusion system for visual tracking. Tracking was performed under democratic cue integration, and the estimated state vector and probability distribution were provided as feedback for adaptive weighting. In this way the algorithm could depend on the appropriate strong cues for a given frame while suppressing unreliable cues. The democratic integration technique was also compared to the popular condensation integration method. These tracking methods developed in the computer vision field focus on natural images or scenes (Brasnett et al., 2007; Moreno-Noguer et al., 2008; Wu and Huang, 2004), for example, pedestrian tracking in a video. So for existing vessel segmentation and

computer vision tracking methods, none are directly applicable to our marginal artery segmentation problem. We cover some of the challenges unique to MA segmentation within this paper (Sec. 3). Because the MA is small in caliber, tortuous in course, and gives rise to innumerable tiny branch vessels, we chose a SMC-based method to track it and thereby reduce false positives.

In this work, we propose a novel Bayesian vessel detection method by fusing multiple cues extracted from CT images to automate the detection of the marginal artery on high-resolution abdominal CT angiograms. In our previous work, cues extracted from CTA were fused using a cue independence assumption under Naïve Bayes methodology (Wang, 2013). Each cue was assigned a weighting parameter to control its impact on the tracking likelihood function. Such a weighting scheme involves parameter learning, making it difficult to introduce new informative cues. In addition, cues may not truly fulfill an independence assumption, especially as several cues are employed and redundancy and dependence exist inevitably. To overcome these problems, in this paper we propose to utilize supervised learning in the probabilistic modeling of a Bayesian tracking framework. For supervised learning we employ a random forest (RF) classifier to intelligently weigh and fuse multiple cues, and we embed the classification confidence score of RF in the tracking framework. We also train a random forest classifier to automate tracking termination and to perform vessel pruning to remove false positives.

3. Tracking challenges

The characteristics and structure of the marginal artery pose several unique and significant challenges to extracting the vessel path with high recall and precision. Several components of our algorithm were developed specifically to handle these challenges, and thus they merit a brief description.

- a) The marginal artery is composed of several large, anastomosing loops of similar diameter (Fig. 1). This causes difficulty for a local, iterative tracking methodology such as sequential Monte Carlo which only has the ability to select a single most probable path. We integrate a robust bifurcation detection step (Sec. 7) in order to achieve high recall of the marginal artery.
- b) In addition to large loops, the marginal artery feeds many smaller straight arteries and vasa recta branches which deliver blood supply to the colon (Fig. 1). These vessels are typically but not always smaller in caliber than the MA, distracting the algorithm from the correct path. (Supplementary file: Fig. S1 shows several straight artery branches perfusing the transverse and descending colon which were automatically tracked by our algorithm.) Learning-based stop criteria (Sec. 8) and pruning method (Sec. 9) minimized these false positives.
- c) The marginal artery makes several connections to major abdominal vessels via the inferior and superior mesenteric artery thereby providing many opportunities to leave the true path. (Supplementary file: Fig. S2 shows an example of over-segmentation of abdominal vasculature of the small bowel which could occur without the appropriate stop criteria and segmentation pruning.)

d) Due to varying blood flow or vessel constriction, some segments of the marginal artery will be poorly enhanced making segmentation difficult (Supplementary file: Fig. S3). In particular, distal segments of the marginal artery such as the region near the splenic flexure and descending colon typically have lower blood flow and are consequently less enhanced. To address this problem, we employ multiple features are employed to achieve robust tracking even in poorly enhanced vessel segments (Sec. 5).

4. Sequential Monte Carlo tracking

First we introduce the sequential Monte Carlo tracking framework and notation.

Observations $\{\mathbf{y}_t; t \in \{1 : T\}\}$, $\mathbf{y}_t \in R^{m_y}$ where $m_y = 8$, are typically captured in a sequential order. Each observation has an associated hidden variable $\{\mathbf{x}_t; t \in \{1 : T\}\}$, $\mathbf{x}_t \in R^{m_x}$ where $m_x = 3$, which generally corresponds to the location of the target at time point t . For each time point t , the observation \mathbf{y}_t is only conditionally dependent on \mathbf{x}_t , i.e. $p(\mathbf{y}_t | \mathbf{y}_{1:t-1}, \mathbf{x}_{1:t}) = p(\mathbf{y}_t | \mathbf{x}_t)$, where $\mathbf{y}_{1:t-1}$ represents all observations from time point 1 to time point $t-1$ and $\mathbf{x}_{1:t}$ represents all hidden variables from time point 1 to time point t . We also assume that the time sequence \mathbf{x}_t , $t=1,2,\dots,T$ has a Markov property of order one: $p(\mathbf{x}_t | \mathbf{x}_{1:t-1}) = p(\mathbf{x}_t | \mathbf{x}_{t-1})$. The dynamics of the Markov chain can be described by the following two steps:

1) Prediction step:

$$p(\mathbf{x}_t | \mathbf{y}_{1:t-1}) = \int p(\mathbf{x}_t | \mathbf{x}_{t-1}) p(\mathbf{x}_{t-1} | \mathbf{y}_{1:t-1}) d\mathbf{x}_{t-1}$$

2) Update step:

$$p(\mathbf{x}_t | \mathbf{y}_{1:t}) = \frac{p(\mathbf{y}_t | \mathbf{x}_t) p(\mathbf{x}_t | \mathbf{y}_{1:t-1})}{p(\mathbf{y}_t | \mathbf{y}_{1:t-1})}$$

In our implementation, the state variable \mathbf{x} was composed of $\mathbf{x} = (x, y, z)$ where x , y , and z are the coordinates of the current tracker location.

4.1. Prediction model using eigenvector field

The majority of vessel segments are smooth in 3D space and exhibit a tubular structure, so a constant velocity model was appropriate at most time points. The constant velocity model captures this smooth translational motion:

$$\mathbf{V}_{t+1} = \mathbf{F}\mathbf{V}_t + \mathbf{d}_t, \quad \mathbf{d}_t \sim N(0, \Sigma_d),$$

where matrix \mathbf{F} controls the speed at which the target (vessel detection) can proceed during the tracking process. \mathbf{d}_t follows a zero-mean Gaussian distribution N . $\mathbf{v} = (x, x', y, y', z, z')$ where x , y , and z are the coordinates of the current location and x' , y' , and z' are components of the moving speed of the tracker. However, some vessel segments change direction abruptly and cannot be captured by a simple translational motion model, especially at vessel bifurcation points. In order to track this movement, we employed a vector field model for motion prediction. A vector field was extracted by eigenvector decomposition of

the Hessian matrix (Sec. 5.2). For eigenvectors (e_1, e_2, e_3), e_3 is the eigenvector associated with the lowest magnitude eigenvalue and indicates the direction of least curvature. This corresponds to the direction along the length of the vessel. Selective eigenvector information was similarly used by Bloch et al. (2010) in vessel tracking on CT angiography and magnetic resonance angiography. In that work, the authors used the e_3 vector to define the normal direction to a cross-section plane for a circular vessel feature. To our knowledge, such an eigenvector field has never been used previously as a prediction model for SMC tracking in medical imaging. Our proposed algorithm jointly uses vector field motion, where the marginal artery turns sharply, and translational motion, which is based on the previous time step. Fig. 3 shows the vector field on a short, curved segment of the marginal artery.

5. Vessel feature cue extraction

In previous Monte Carlo vessel detection work on CT (Florin et al., 2005; Schaap et al., 2007), intensity is used as the primary source of information. Upon visual inspection of CT images for vessel detection, radiologists not only observe intensity, but also utilize spatial information, such as organ location, proximity of surrounding fat and muscle, and the smooth, continuous, tubular structure of vessels. Thus, human vision combines multiple cues to identify and track vessels. Inspired by this intuitive method used by radiologists, in this work we propose a new likelihood model for vessel detection by fusing multiple cues. (Supplementary file: Fig. S4 shows four tracking features overlaid on an axial CT image.)

5.1. Intensity cue

As with traditional vessel detection methods, intensity is the most important information for vessel tracking on CT, and the basis of derivation of all other cues. CT scans are performed with arterial phase intravenous contrast, and the vessel appears bright against a dark background. For a particle \mathbf{x}_t at time point t , we extracted a spherical search region (radius of 2 voxels) centered on the particle location. The summation of the intensity of all voxels within the sphere was used as a composite cue for tracking.

5.2. Vessel response cue

Because short, local vessel segments typically exhibit tubular structure, a vesselness cue is extremely beneficial to differentiate true vessels from noisy blob-like areas also enhanced by contrast agent or organ boundaries. We employed a 3D multiscale vessel enhancement filter described in Li *et al.* (2003) to provide this vesselness measurement. Li *et al.* claim that this method was able to enhance line structures while suppressing responses from other shapes which led to improved specificity when compared to other methods. Vessel response is formulated as follows,

$$vesselness(\lambda_1, \lambda_2, \lambda_3) = \begin{cases} \frac{\sigma^2 |\lambda_2| (|\lambda_2| - |\lambda_3|)}{|\lambda_1|}; & < 0, \lambda < 0 \\ 0; & otherwise \end{cases}$$

where σ is the Gaussian filter scale and $|\lambda_1| > |\lambda_2| > |\lambda_3|$ are the three eigenvalues extracted by eigenvector decomposition of the Hessian matrix,

$$H = \begin{vmatrix} f_{xx} & f_{xy} & f_{xz} \\ f_{yx} & f_{yy} & f_{yz} \\ f_{zx} & f_{zy} & f_{zz} \end{vmatrix}$$

where f is the 3D image volume. Frangi *et al.* (1998) state that the condition for 3D bright tubular structure against a dark background is $\lambda_1 \approx \lambda_2 \ll \lambda_3 \approx 0$. For the Gaussian filter, spatial scale standard deviations from 0.5 voxels to 2 voxels with 0.25 voxel incremental steps were used in multi-scale analysis. The maximum vesselness response across all scales was used as a feature.

5.3. Ray casting cue

Organs abutting the marginal artery are a major source of false positives. Organ boundaries frequently have a non-zero Hessian vesselness response due to partial line or curve character, and can mislead the algorithm from the true marginal artery path. Vessels relatively larger in caliber or following a relatively straight trajectory compared to the MA, such as the aorta or renal vessels, also provide an opportunity for the algorithm to track into other areas of the abdomen. To avoid these particle tracks, we employed a 3D ray casting technique and applied it at each particle. Rays were cast in 26 spatial directions and stop when reaching either low intensity or a maximum distance, both determined heuristically. Particles received a ray casting score, which was the sum of the 26 ray lengths. High scores indicated false positives such as an organ or large bore vessel.

5.4. Maximum intensity projection cue

Maximum intensity projection (MIP) provides a method to amplify intensity signal in a selected direction. This is an informative cue for noisy data and thin, non-continuous, peripheral vessel segments with poor contrast enhancement. A MIP was calculated during the feature extraction phase based on the three projection directions of the transverse, sagittal, and coronal planes. Overlapping 16 mm slabs were used to construct 2D images and vessel enhancement filters generated detections. We then projected the 2D detections back to 3D space to create a binary mask. More information about this feature is available in Zhang *et al.* (2013). The sum of binary mask voxels within the spherical search region was used as a vessel tracking cue. This feature was sensitive to not only the marginal artery but also numerous small branch vessels.

5.5. Spanning tree cue

Due to poor contrast enhancement, some vessel segments are not well distinguished by either intensity or vesselness cues alone, which requires regional context information to track vessels. We employed a minimum spanning tree algorithm to connect segments with very high vesselness response. We utilized intensity or vesselness values to determine the weight of a node in the spanning tree. High vesselness values play the dominant role in extracting the marginal artery except in the image regions with vesselness values of zero. If we purely used vesselness in these regions, the spanning tree would choose random image points because the weights of all nodes were equal. In these regions, we used the image

intensity values for the nodes' weights, and the spanning tree picked image points with high intensity values as the artery candidates. By combining intensity and vesselness, we guide the minimum spanning tree to reconstruct the marginal artery subgraph.

6. Vessel prediction during tracking by cue fusion

In recent years, random forest classifiers have developed as a fast and accurate ensemble learning technique, and have also been used to integrate multiple cues for target tracking (Shi, 2011). As an additional method for comparison to the cue fusion vessel likelihood function, we leveraged a random forest classifier to weigh cue information and make tracking decisions.

In a seminal paper, Breiman (2001) defines a random forest classifier as a composition of many tree-structured classifiers, each of which cast a vote for classification of a given input vector \mathbf{y}_t . To generate a classifier tree $h(\mathbf{y}_t, \theta)$ in a random decision forest, a vector θ is selected at random from training data having K features. Tree h is then grown as a hierarchy of nodes with a root (vector input) node and terminal leaf nodes holding the final prediction for that tree. At each node in the decision tree, a feature split is optimized to partition the data into two subsequent branches. For an observed input vector \mathbf{y}_t during tracking, the information works its way from the root node to a terminal leaf node to make the prediction for that vector. Each tree in the forest is generated independently and at random by selecting a subset of features and training data. For random forest regression, the prediction given input \mathbf{y}_t is continuous and made by taking an average of decisions from all trees in the forest.

Random forests are rapidly trained and tested and therefore are adept at learning on large-scale datasets, such as datasets used in medical imaging. Compared with state-of-the-art kernel based learning methods, random forests showed comparable performance, better scale-up ability and require much less memory space. Random forests are also very robust to outliers and noise. Random forest regression has been used previously by Criminisi et al. (2010) for anatomical detection. Our random forest implementation was from the work of Abhishek Jaiantilal (<https://code.google.com/p/randomforest-matlab/>), and was applied to the vessel prediction step, termination decision making, and vessel pruning. For vessel tracking, a random forest with 50 trees was trained on the eight vessel cues as described above (Sec. 5). The positive samples were the ground truth segmentations from the 10 training patients. The negative samples were randomly selected from an area within 20 mm of the ground truth. The parameter *mtry*, the number of predictors sampled for splitting at each decision node, was set to 2. The number of trees and the number of predictors sampled for splitting at each node were selected empirically based on the performance of the random forest on the manually labeled training data. The random forest input is a feature vector describing a voxel and the output is a continuous confidence score ranging from -1 to $+1$ indicating whether or not the voxel belongs to the marginal artery. This input-output strategy is also used in the other termination and pruning random forests.

7. Automatic bifurcation detection

Two techniques are commonly used to robustly identify bifurcation. One method by Allen et al. (2008) used k-means particle clustering at each step of vessel segmentation. The other

method samples voxels from a spherical shell at each step and has previously been used for detecting bifurcations in airway tree segmentation (Xiong et al., 2012). To handle our abdominal vessel bifurcation problem, we implemented an automatic bifurcation detection system using the spherical shell technique due to its demonstrated robustness. At each step, the shell with a radius of 2 voxels was sampled. The features for each voxel in this shell are fed to the random forest vessel detector and connected component analysis is performed to find patches of high vessel confidence. A single vessel path entering and leaving the shell produces two high confidence patches. A bifurcation will cause three patches of high confidence (Fig. 4). In the latter case, multiple parallel particle filter paths were initialized to complete the vessel tree.

8. Termination checking

The marginal artery's meandering course, numerous branch vessels, broad geographic span, and proximity to other abdominal organs present substantial challenges to tracking and segmenting with high precision. In addition to a robust tracking algorithm and bifurcation detection system, robust self-termination criteria are necessary to prevent tracking onto alternate vessels and organs. To determine if a tracked segment diverged from the vasculature, a random forest classifier was trained using the 10 training patients. Positive samples were the ground truth segmentations. Negative samples were randomly chosen from a region surrounding the ground truth. The training data was balanced with 50 percent positive and 50 percent negative samples, with a total of 350,000 samples. The trained random forest used 100 trees and selected from a subset of 5 of the 25 features at each tree node. Besides the vessel cues mentioned previously (Sec. 5), the vessel terminating random forest had a few additional features:

- a) Low intensity histogram: Segmented paths frequently follow bifurcations to small branches supplying blood flow directly to the colon (Figs. 1 and S1 in supplementary file). This results in indefinite tracking along the colon. For this reason, at each step the local region is examined for ultra low intensity information, indicating patches of air within the bowel. A histogram of all values below -224 HU with bins of 50 HU was used to train the random forest classifier for termination decision making. The path self-terminates when identifying a low-intensity region of air in close proximity.
- b) Region growing: The marginal artery is unique relative to surrounding vasculature and tissue with respect to its thinness and relatively uniform intensity. Thus, at each step a region growing algorithm is performed limited by distance (7 mm) and percentile change in intensity (3.5%). The total percentage of a 7 mm radius sphere filled by region growing at each step was used for the termination cue. By this technique tracks are terminated when reaching large-bore arteries or veins, or structures such as the kidney, stomach, and liver.
- c) Kernel density estimators: In our previous work (Wang, 2013), we used kernel density estimation to build probability density functions (PDF) for each cue. We continue using these features in vessel termination; however, instead of fusing the probability density as a product of likelihoods, we feed the values to the more advanced random forest learning algorithm. PDFs were built using features extracted from the

segmentations of the 10 patient training set. Fig. S5 shows the estimated probability density function for each feature.

As a means of preventing false positives, bifurcation branching level information was collected and used to limit the extent of vessel tree development. The maximum number of branching levels (not the number of possible branches) was set to 5. After reaching this level limit, tracking was terminated to prevent excessive tracking of the abdominal vasculature. Fig. S6 shows an illustration of branching levels, with each level labeled in a different color. Lastly, if the vessel tracker reached an image voxel that had been previously visited, the tracker was terminated to prevent redundant segmentation.

9. Vessel segmentation pruning

Due to the high vascularity of the mesentery and the robustness of the bifurcation detector, many undesired vessel branches were segmented by the SMC vessel tracker. These smaller vessels were not included in the marginal artery ground truth labels, which resulted in low precision values. The most problematic vessels were the aorta, common iliac arteries, and the straight arteries [Fig. 1, Fig. S1 (supplementary file), and Fig. S6 (supplementary file)]. In order to remove the false positives segmented by the vessel tracker, we trained a random forest pruning algorithm using the 10 patients in the training set.

The random forest was trained using the previously described vessel cues: intensity, vesselness response, ray casting, MIP, and spanning tree (Sec. 5). These features provide information about whether the voxel is part of a vessel, but they cannot distinguish between abdominal vessels and the desired marginal artery. To make this distinction, the random forest was trained with additional location information. We supplement the vessel cues with normalized coordinate location, Hessian eigenvectors, distance from user-generated seed points, and proximity to the colon.

Because the marginal artery closely follows the curvature of the colon, we approximated the location of the colon for each patient through the use of a colon probability map. Although the images used in our experiment were CT angiograms, we were still able to effectively use a probability map created using 66 colon centerlines labeled on CT colonography (CTC) data. Each centerline was registered to a target centerline using the iterative closest point (ICP) algorithm (Rusinkiewicz and Levoy, 2001). The centerlines were dilated, summed, smoothed with a Gaussian filter, and normalized. The ICP algorithm was next used to automatically align the completed probability map to each patient's abdominal gas bubbles, mainly located in the colon, which were simply segmented by intensity thresholding. In a clinical application of our marginal artery segmentation framework to CTC images, segmentation of the majority of the colon would be achievable. Those segmentations could be used alone to register a colon probability map or jointly with the colonic gas bubbles. One of the goals of marginal artery segmentation is to provide a guide for better connecting collapsed segments of the colon. The colon probability map works in a similar fashion, providing a rudimentary guide for marginal artery segmentation in sections where the colon is difficult to locate. The marginal artery is a much more precise coordinate system for colon segmentation. (Supplementary file: the result of this probability map registration is visualized in Fig. S7.)

The random forest utilized 250 decision trees and selected from a random subset of 5 image features at each decision node. The positive training samples were the ground truth segmented voxels of the marginal artery. The negative voxels were randomly selected from areas near the ground truth, near the MIP mask, or near image intensities greater than -24 HU. Positive samples were duplicated 10 times in order to achieve a balanced training set with a significant number of negative training samples. This was done in order to encompass the large variability of the negative samples. This sampling strategy resulted in 838,060 training samples taken from the 10 patients in the training set. As expected, the feature importance determined by the random forest shows that the location-based features were more important than the vessel features in distinguishing unwanted abdominal vessels from the marginal artery (Fig. S8). When the random forest pruning algorithm was applied to the vessel segmentation results created by the SMC tracker, we were able to remove a significant amount of false positives with only a minor drop in recall rate. Performance of the pruning algorithm is shown visually in Fig. 5 and is quantified in the experimental results (Sec. 11) and supplemental data (Fig. S7 and Table S1).

10. Evaluation

10.1. Dataset

Data acquisition and analysis were conducted under an Institutional Review Board (IRB) approved protocol. Dataset contained 40 high-resolution contrast-enhanced abdomen and pelvis CT angiograms performed or evaluation of small bowel carcinoid. Scanning protocol required oral administration of 3 bottles Volumen, intravenous administration of 130 mL Isovue-300 with 5 mL/s injection rate and 30 second delay, and supine patient positioning. Scanning parameters included section collimation of 1.0 mm, reconstruction interval of 0.5 mm, and in-plane pixel dimensions ranging from 0.82-0.94 mm.

10.2. Dataset processing

The ground truth used for training and evaluating our detection algorithm was generated by manual labeling. Manual labeling of the marginal vessels was performed by both a trained computer scientist and a board-certified radiologist using Fiji/ImageJ software with the Simple Neurite Tracer tool (Longair et al., 2011; Schneider et al., 2012). Given the extreme proximity of the marginal artery and vein which precluded the differentiation between artery and vein, a single label for either vessel was deemed sufficient. The marginal vessels coursing along the ascending colon were not manually labeled due to their uniformly poor enhancement which was in part due to the fact that the dataset's CT examination protocol was not specifically designed for visualization of the marginal vessels. The consensus between the two readers established a single ground truth label. Random forest algorithm training was performed on 10 of 40 CT examinations. The remaining 30 of 40 CT examinations composed the test set.

Three manual seed points were designated at the junctions between the transverse and descending colon segments of the marginal artery and the SMA and IMA. One of the seed points was placed in the middle at the splenic flexure. Tracking computational time was approximately 2-3 hours per patient, and the algorithm was implemented in Matlab version

8.0 on a Dell Precision T7500 work station with 24 GB memory (X5690 Xeon CPU). The NIH Biowulf Linux cluster (biowulf.nih.gov) was utilized to perform parallel computation during tracking. Two factors in the algorithm accounted for the bulk of the processing time: the execution of local region growing at each step to evaluate for path termination, and the robustness of our bifurcation detection system which generates many potential new tracking paths.

10.3. Baseline comparison methods

Two baseline methods were employed in this study. One was a traditional Hessian vessel enhancement filtering method (Li et al., 2003) and the other utilizes the sequential Monte Carlo (SMC) framework with intensity and vesselness as the only features. These methods are referred to as “Hessian Baseline” and “2 Cue Baseline” throughout this text. The Hessian Baseline method consists of segmentation results from thresholding Li’s vessel enhancement filtering response. No manual seed points or tracking framework were used. The threshold was 30. Vessel enhancement filtering was described in Sec. 5.2.

The 2 Cue Baseline used the same sequential Monte Carlo (SMC) tracking framework presented in Sec. 4. It utilized bifurcation detection and experimentally determined stop criteria presented in our previous work (Wang, 2013). However, the key difference was the limited features available to the tracker. The 2 Cue Baseline method used the fusion of two vessel tracking cues as a product of likelihoods:

$$L(y_t|x_t) = L_I(y_t|x_t) \times L_V(y_t|x_t),$$

where L is the probability density function constructed using kernel density estimators (KDE). Features were the summation of intensity and the summation of vesselness within a spherical search region centered on the candidate voxel. Each cue was given equal weight. Cues were taken to be independent, which is a common assumption made in computer vision for a Naïve Bayes’ methodology (Brasnett et al., 2007; Moreno-Noguer et al., 2008). During the tracking prediction step, the cue observations made for each particle were weighted probabilistically using each KDE function and each particle’s vessel likelihood was generated. This likelihood was used to update the tracker location.

10.4. Measures of performance

The performance of the algorithm was evaluated by the metrics of recall and precision. Recall was defined as the fraction of ground truth voxels detected by the algorithm, and precision was defined as the fraction of detected voxels that were true detections. A segmented voxel was considered a true positive detection if it was within 5 mm of a ground truth label. This adjusted for the low probability of segmented voxels overlapping and led to rational metrics:

$$Recall = \frac{|\{Reader1 \cap Reader2\} \cap \{segmentation\ results\}|}{|\{marginalartery\}|}$$

$$Precision = \frac{|\{Reader1 \cup Reader2\} \cap \{segmentation\ results\}|}{|\{segmentation\ results\}|}$$

The performance of a method can be difficult to ascertain. An increase in recall is often coupled with a decrease in precision. Adjusting each method to achieve a target performance metric in order to compare the other metrics is an impossible task due to the large variability in the patient images. Because both the recall and precision of the vessel tracker are important, the method's accuracy was measured using a balanced F_1 score. The metric is defined as the harmonic mean:

$$F_1 \text{ score} = 2 \times \frac{Recal \times Precision}{Recall + Precision}$$

11. Experimental results

When determining the accuracy or practicality of a computer-aided detection (CAD) system, sometimes the performance metrics cannot capture the whole story. It is critical to have a deep understanding the advantages and disadvantages of different methods. Visual inspection convincingly demonstrates the importance of a method having both high recall and high precision. Fig. 6 shows results for all four methods on three different patients. These figures confirm why the added complexity of a multi-cue vessel tracker is necessary. The Hessian Baseline results had excellent recall because essentially all the abdominal vasculature was segmented. On the other hand, the 2 Cue Baseline approach had excellent precision because hardly any vasculature was segmented due to the limited number of image cues and simple cue fusion technique. Clearly a balanced approach was needed if the marginal artery of the colon was to be segmented for clinical use as a coordinate system for CT colonography.

In comparing our proposed method with other possible approaches to vessel segmentation (Fig. 7), we demonstrate that our Hessian Baseline method with very high recall (81.6%) and a 2 Cue Baseline method with very high precision (78.1%). A successful vessel segmentation framework should simultaneously approach the high performance metrics set by both of these baseline methods. Our proposed multi-cue random forest sequential Monte Carlo (RF SMC) algorithm with vessel pruning achieved an average recall rate of 67.7% and an average detection precision to 75.2%. These metrics were not statistically significantly different from the best metrics set by the baselines. The recall values for both RF SMC methods were statistically significantly higher than the recall of the 2 Cue Baseline method. Also, the precision values for both RF SMC methods were statistically significantly higher than the precision of the Hessian Baseline method. Importantly, the F_1 score of all pairs of methods were statistically significantly different. Fig 8 shows the comparison of the F_1 score for each method. Finally, Table 1 summarizes the results for statistical significance testing of all pair-wise comparisons. Significance was determined with an overall $\alpha=0.05$ using a paired t-test with a Bonferroni correction to control for familywise errors resulting from

multiple comparisons. [A table with all performance metrics for each patient is included in the supplemental data (Table S1).]

12. Discussion

Here we present a novel Bayesian tracking framework using sequential Monte Carlo and multiple cue fusion to segment the marginal vessels of the colon on contrast-enhanced CT angiograms. By using multiple cue fusion of local and global information, we achieve an average recall of $67.7 \pm 26.2\%$ (one standard deviation) and precision of $75.2 \pm 15.5\%$. These results represent significantly superior results compared to baseline Hessian analysis, whose average recall and precision are $81.6 \pm 20.2\%$ and $2.7 \pm 1.1\%$ respectively. Tracking with 2 cues as an alternative baseline method provided a recall of only $30.7 \pm 18.6\%$, indicating the significant benefit of including a greater number of cues for more robust tracking. Importantly, each of our proposed methods showed a statistically significant increase in the F_1 score when compared to the traditional Hessian vesselness method. Furthermore, we compare this work with our previous results published in Wang et. al. (2013), which achieved an average F_1 score of $32.1 \pm 14.9\%$ on a testing set consisting of seven patients. On those seven patients, our sequential Monte Carlo tracker using random forest achieved an average F_1 score of $51.5 \pm 9.2\%$ (paired t-test, $p < 0.05$) without vessel pruning and 75.5 ± 11.9 (paired t-test, $p < 0.05$) with vessel pruning. These seven patients were well-suited for the KDE cue-fusion framework used in Wang et. al. (2013); however, the random forest-based cue fusion presented here made the tracker much more consistent and robust on a testing set that is 4-fold larger.

The vessel pruning procedure which took advantage of the marginal artery and colon location showed statistically significant improvement in precision and F_1 score compared to our sequential Monte Carlo tracker using random forest without post-processing. This demonstrates the usefulness of post-processing procedure after vessel tree generation.

One of the primary limitations of this work is the systematically elevated false positive detections due to the vasa recta and straight arteries of the transverse colon. This geographic discrepancy of false positives within the transverse versus descending colon can be in part explained from an innate anatomic feature of the vasa recta; the vasa recta of the transverse colon are more numerous and frequent in the transverse colon, spaced less than 1 cm apart within the transverse colon within extensive collateral branches in comparison to the descending colon where vasa recta are spaced 2 cm apart with fewer collateral branch vessels (Allison et al., 2010). To address this systematic problem, we first consider an overgrown vessel tree followed by a structural pruning scheme, which has been shown to be an effective means of false positive reduction (Kaufhold et al., 2012; Lu et al., 2009a). Our tracing method serves well as a pre-stage of focusing on the tracking efficiency using local image features and contexts and high recall on vessel detection. The higher false positive rate caused by tracking can be tackled by robust structural pruning and linking techniques (Kaufhold et al., 2012; Lu et al., 2009a) since more global vessel branch level features can be used to build a complementary statistical model on vessel shape and geometry. This can understand the geometrical structure of different branches on the vessel tree. For the stopping criterion to prevent tracing into too fine vasculature near the colon, the vessel

lumen radius, volume-to-length ratio features can also be effective, as in (Lu et al., 2009b) to distinguish finer small intestine segments from colon segments in colon segmentation.

Our previous work (Wei et al., 2013) demonstrated the feasibility of using a marginal artery segmentation to aid CT colonography (CTC) in two ways. Firstly, the alignment of the vessel with the colon can assist supine-prone registration of the colonic polyps. Secondly, the vessel can help properly connect collapsed segments of the colon. Here, our method has been validated on a non-CTC dataset in which many sections of the colon are collapsed or constricted, because the colon is not insufflated with air during bowel preparation. Sequential Monte Carlo tracking with random forest and vessel pruning shows potential usefulness in CTC, although the lack of intravenous contrast in CTC will need to be addressed. In contrast to the work of Wei et al., where the marginal artery was segmented manually, this manuscript demonstrates semi-automated segmentation of the marginal artery of the colon.

Segmenting the marginal artery of the colon is a challenging task. We overcame several obstacles during the development of the framework presented here. The looping and branching nature of the marginal artery makes sequentially tracking the vessel difficult (Figs. 1 and S1 in supplementary file). To address this problem, we developed a robust bifurcation technique to add branches to the segmentation (Fig. 4). Also, the marginal artery is connected to a large network of abdominal vessels which a vessel tracker can enter and cause extreme over-segmentation (Fig. S2 in supplementary file). We developed a vessel pruning technique and a termination check, both using random forest, in order to remove false positives and prevent over-segmentation (Fig. 5). Finally, a constricted blood supply to segments of the marginal artery and inconsistent imaging contrast can make tracking difficult. We utilized a method that can fuse information from multiple image cues into a vessel prediction in order to track the marginal artery with high recall.

Embedding machine learning techniques such as discriminative feature extraction and random forest classification in the vessel segmentation framework is a key contribution of the work presented in this paper. In the field of medical image analysis, the majority of work on vessel segmentation from radiological images focuses on modeling the appearance and structure of vessels (Lesage et al., 2009). Very few works have adopted a similar strategy to ours to solve the vessel segmentation problem. To name a few, Maiora et al. proposed an active learning mechanism for abdominal aortic aneurysm thrombus segmentation in CTA image (Maiora et al., 2014). They employed random forest to classify voxels based on intensity features extracted from the 2D neighborhood of a voxel. Ricci and Perfetti employed support vector machine (SVM) for retinal blood vessel segmentation from digital fundus imaging (Ricci and Perfetti, 2007). Similarly, Zuluaga et al. also employed SVM to detect abnormal vascular cross-sections in CT images (Zuluaga et al., 2011). Schaap et al. proposed a coarse-to-fine method to segment coronary arteries in CTA (Schaap et al., 2011). In the refinement stage, segmentation of vessel boundary is improved by non-linear regression. Cross-sectional intensity profiles around the vessel were extracted and fed to a regressor. In these works and ours, the proposed methods utilized classification techniques to solve various aspects of the vessel segmentation problems. However, they employed simple features like intensity profile whereas our method extracts more discriminative features from each voxel such as probability density functions, spanning tree and vessel

response cues. In addition, our classification module is seamlessly integrated with the SMC dynamic tracking framework. For other methods, vessel segmentation usually was derived directly from classification results after certain post-processing such as thresholding or morphological operations.

In conclusion, we demonstrated that near-complete automation of marginal vessel segmentation is indeed feasible, and by doing so we present a supplementary spatial coordinate system for colon segmentation when this task has been confounded by lumen collapse. The significance of this work is two-fold. First, there has been no precedent for automated segmentation of this anatomic structure to date. Second, in the same manner Zhang et. al. (2012a; 2012b) showed how mesenteric vascular detection could be applied to automated small bowel segmentation, we demonstrate how to segment the colonic vasculature which can serve as a geometric scaffold by which to navigate the colon. We have made strides towards automating segmentation of a very challenging vessel within the abdomen that has application in the fields of CT colonography and colonic polyp detection.

Supplementary Material

Refer to Web version on PubMed Central for supplementary material.

Acknowledgements

This work was supported by the Intramural Research Programs of the NIH Clinical Center and by a Cooperative Research and Development Agreement with iCAD. This study utilized the high-performance computational capabilities of the Biowulf Linux cluster at the National Institutes of Health. We thank Dr. Steven Wank for patient referral. We also thank the anonymous reviewers for their constructive comments which helped improve the manuscript.

Bibliography

- Allison AS, Bloor C, Faux W, Arumugam P, Widdison A, Lloyd-Davies E, Maskell G. The angiographic anatomy of the small arteries and their collaterals in colorectal resections: some insights into anastomotic perfusion. *Annals of surgery*. 2010; 251:1092–1097. [PubMed: 20485132]
- Bloch I, Cesar R Jr, Macedo MG, Mekkaoui C, Jackowski M. Vessel Centerline Tracking in CTA and MRA Images Using Hough Transform. *Progress in Pattern Recognition, Image Analysis, Computer Vision, and Applications*. 2010; 6419:295–302.
- Brasnett P, Mihaylova L, Bull D, Canagarajah N. Sequential Monte Carlo tracking by fusing multiple cues in video sequences. *Image and Vision Computing*. 2007; 25:1217–1227.
- Breiman L. Random forests. *Mach Learn*. 2001; 45:5–32.
- Chen SC, Lu DSK, Hecht JR, Kadell BM. CT colonography: Value of scanning in both the supine and prone positions. *American Journal of Roentgenology*. 1999; 172:595–599. [PubMed: 10063842]
- Criminisi, A.; Shotton, J.; Robertson, D.; Konukoglu, E. Regression Forests for Efficient Anatomy Detection and Localization in CT Studies. In: Menze, B.; Langs, G.; Tu, Z.; Criminisi, A., editors. MICCAI. Springer-Verlag; Berlin, Heidelberg, Beijing, CN: 2010. p. 106-117.
- Dachman AH, Obuchowski NA, Hoffmeister JW, Hinshaw JL, Frew MI, Winter TC, Van Uiter RL, Periaswamy S, Summers RM, Hillman BJ. Effect of computer-aided detection for CT colonography in a multireader, multicase trial. *Radiology*. 2010; 256:827. [PubMed: 20663975]
- Florin, C.; Paragios, N.; Williams, J. MICCAI. Springer-Verlag; Berlin, Heidelberg, Palm Springs, US: 2005. Particle filters, a quasi-monte carlo solution for segmentation of coronaries; p. 246-253.
- Frangi, AF.; Niessen, WJ.; Vincken, KL.; Viergever, MA. MICCAI. Springer-Verlag; Berlin, Heidelberg, Cambridge, US: 1998. Multiscale vessel enhancement filtering; p. 130-137.

- Friman O, Hindennach M, Kühnel C, Peitgen H-O. Multiple hypothesis template tracking of small 3D vessel structures. *Medical Image Analysis*. 2010; 14:160–171. [PubMed: 20060770]
- Halligan S, Mallett S, Altman DG, McQuillan J, Proud M, Beddoe G, Honeyfield L, Taylor SA. Incremental benefit of computer-aided detection when used as a second and concurrent reader of CT colonographic data: multiobserver study. *Radiology*. 2011; 258:469–476. [PubMed: 21084409]
- Hampshire, T.; Roth, H.; Hu, M.; Boone, D.; Slabaugh, G.; Punwani, S.; Halligan, S.; Hawkes, D. MICCAI. Springer-Verlag; Berlin, Heidelberg, Toronto, CA: 2011. Automatic prone to supine haustral fold matching in CT colonography using a Markov random field model; p. 508-515.
- Johnson CD, Chen M-H, Toledano AY, Heiken JP, Dachman A, Kuo MD, Menias CO, Siewert B, Cheema JI, Obregon RG. Accuracy of CT colonography for detection of large adenomas and cancers. *New England Journal of Medicine*. 2008; 359:1207–1217. [PubMed: 18799557]
- Allen K, Noble JA. A Recursive, Stochastic Vessel Segmentation Framework that Robustly Handles Bifurcations. *Proceedings of Medical Image Understanding and Analysis*. 2008 C.Y.
- Kaufhold JP, Tsai PS, Blinder P, Kleinfeld D. Vectorization of optically sectioned brain microvasculature: Learning aids completion of vascular graphs by connecting gaps and deleting open-ended segments. *Medical Image Analysis*. 2012; 16:1241–1258. [PubMed: 22854035]
- Kristan M, Pers J, Perse M, Kovacic S. Closed-world tracking of multiple interacting targets for indoor-sports applications. *Computer Vision and Image Understanding*. 2009; 113:598–611.
- Lacoste, C.; Finet, G.; Magnin, IE. Coronary tree extraction from X-ray angiograms using marked point processes. *IEEE International Symposium on Biomedical Imaging*; IEEE; 2006. p. 157-160.
- Lesage D, Angelini ED, Bloch I, Funka-Lea G. A review of 3D vessel lumen segmentation techniques: Models, features and extraction schemes. *Medical Image Analysis*. 2009; 13:819–845. [PubMed: 19818675]
- Li Q, Sone S, Doi K. Selective enhancement filters for nodules, vessels, and airway walls in two- and three-dimensional CT scans. *Medical Physics*. 2003; 30:2040–2051. [PubMed: 12945970]
- Longair MH, Baker DA, Armstrong JD. Simple Neurite Tracer: open source software for reconstruction, visualization and analysis of neuronal processes. *Bioinformatics*. 2011; 27:2453–2454. [PubMed: 21727141]
- Lu, L.; Bi, J.; Yu, S.; Peng, Z.; Krishnan, A.; Zhou, XS. Hierarchical learning for tubular structure parsing in medical imaging: A study on coronary arteries using 3D CT Angiography; *IEEE International Symposium on Computer Vision*; IEEE; 2009a. p. 2021-2028.
- Lu, L.; Wolf, M.; Liang, J.; Dundar, M.; Bi, J.; Salganicoff, M. MICCAI. Springer-Verlag; Berlin, Heidelberg, London, UK: 2009b. A two-level approach towards semantic colon segmentation: removing extra-colonic findings; p. 1009-1016.
- Maiora J, Ayerdi B, Grana M. Random forest active learning for AAA thrombus segmentation in computed tomography angiography images. *Neurocomputing*. 2014; 126:71–77.
- Moreno-Noguer F, Sanfeliu A, Samaras D. Dependent multiple cue integration for robust tracking. *Ieee Transactions on Pattern Analysis and Machine Intelligence*. 2008; 30:670–685. [PubMed: 18276972]
- Pickhardt PJ, Choi JR, Hwang I, Butler JA, Puckett ML, Hildebrandt HA, Wong RK, Nugent PA, Mysliwiec PA, Schindler WR. Computed tomographic virtual colonoscopy to screen for colorectal neoplasia in asymptomatic adults. *New England Journal of Medicine*. 2003; 349:2191–2200. [PubMed: 14657426]
- Ricci E, Perfetti R. Retinal blood vessel segmentation using line operators and support vector classification. *Ieee Transactions on Medical Imaging*. 2007; 26:1357–1365. [PubMed: 17948726]
- Roth HR, McClelland JR, Boone DJ, Modat M, Cardoso MJ, Hampshire TE, Hu M, Punwani S, Ourselin S, Slabaugh GG. Registration of the endoluminal surfaces of the colon derived from prone and supine CT colonography. *Medical Physics*. 2011; 38:3077. [PubMed: 21815381]
- Rusinkiewicz, S.; Levoy, M. *Proceedings of 3-D Digital Imaging and Modeling*. IEEE; 2001. Efficient variants of the ICP algorithm; p. 145-152.
- Schaap, M.; Manniesing, R.; Smal, I.; Van Walsum, T.; Van Der Lugt, A.; Niessen, W. MICCAI. Springer-Verlag; Berlin, Heidelberg, Brisbane, AU: 2007. Bayesian tracking of tubular structures and its application to carotid arteries in CTA; p. 562-570.

- Schaap M, van Walsum T, Neeffjes L, Metz C, Capuano E, de Bruijne M, Niessen W. Robust Shape Regression for Supervised Vessel Segmentation and its Application to Coronary Segmentation in CTA. *Ieee Transactions on Medical Imaging*. 2011; 30:1974–1986. [PubMed: 21708497]
- Schneider CA, Rasband WS, Eliceiri KW. NIH Image to ImageJ: 25 years of image analysis. *Nat Methods*. 2012; 9:671–675. [PubMed: 22930834]
- Shi, X.; Zhang, X.; Liu, Y.; Hu, W.; Lin, H. Multi-cue based multi-target tracking using online random forests; *IEEE International Conference on Acoustics, Speech, and Signal Processing*; Prague, CZ. 2011. p. 1185-1188.
- Siegel, R.; Naishadham, D.; Jemal, A. Cancer statistics. Vol. 63. *A Cancer Journal for Clinicians*; CA: 2013. 2013. p. 11-30.
- Spengler M, Schiele B. Towards robust multi-cue integration for visual tracking. *Machine Vision and Applications*. 2003; 14:50–58.
- Summers RM, Yao JH, Pickhardt PJ, Franaszek M, Bitter I, Brickman D, Krishna V, Choi JR. Computed tomographic virtual colonoscopy computer-aided polyp detection in a screening population. *Gastroenterology*. 2005; 129:1832–1844. [PubMed: 16344052]
- Wang, S.; Peplinski, B.; Lu, L.; Zhang, W.; Liu, J.; Wei, Z.; Summers, RM. Sequential Monte Carlo Tracking for Marginal Artery Segmentation on CT Angiography by Multiple Cue Fusion. In: Mori, K.; Sakuma, Ichiro; Sato, Toshinobu; Barillot, Christian; Navab, Nassir, editors. *MICCAI*. Springer-Verlag; Berlin, Heidelberg, Nagoya, JP: 2013.
- Wang S, Petrick N, Van Uitert RL, Periaswamy S, Summers RM. 3D supine and prone colon registration for computed tomographic colonography scans based on graph matching. *Proceedings of SPIE: Medical Imaging*. 2011:79631F.
- Wei Z, Yao J, Wang S, Liu J, Dwyer AJ, Pickhardt PJ, Nowinski WL, Summers RM. Feasibility of the Marginal Artery as a Complementary Colon Coordinate System for CT Colonography. 2013 In Press in *American Journal of Roentgenology*.
- Wu Y, Huang TS. Robust visual tracking by integrating multiple cues based on co-inference learning. *Int J Comput Vision*. 2004; 58:55–71.
- Xiong GL, Chen CZ, Chen JZ, Xie YQ, Xing L. Tracking the motion trajectories of junction structures in 4D CT images of the lung. *Physics in Medicine and Biology*. 2012; 57:4905–4930. [PubMed: 22796656]
- Yee J, Kumar NN, Hung RK, Akerkar GA, Kumar PR, Wall SD. Comparison of Supine and Prone Scanning Separately and in Combination at CT Colonography 1. *Radiology*. 2003; 226:653–661. [PubMed: 12601201]
- Zhang W, Liu J, Yao J, Nguyen T, Louie A, Wank S, Summers RM. Computer-aided mesenteric small vessel segmentation on high-resolution 3D contrast-enhanced CT angiography scans. *Proceedings of SPIE: Medical Imaging*. 2012a:63.
- Zhang, W.; Liu, J.; Yao, J.; Nguyen, TB.; Louie, A.; Wank, S.; Nowinski, WL.; Summers, RM. Mesenteric vasculature-guided small bowel segmentation on high-resolution 3D CT angiography scans; *IEEE International Symposium on Biomedical Imaging*; IEEE; 2012b. p. 1280-1283.
- Zhang WD, Liu JM, Yao JH, Louie A, Nguyen TB, Wank S, Nowinski WL, Summers RM. Mesenteric Vasculature-Guided Small Bowel Segmentation on 3-D CT. *IEEE Trans. Med. Imaging*. 2013; 32:2006–2021. [PubMed: 23807437]
- Zhou SHK, Chellappa R, Moghaddam B. Visual tracking and recognition using appearance-adaptive models in particle filters. *IEEE Transactions on Image Processing*. 2004; 13:1491–1506. [PubMed: 15540457]
- Zuluaga MA, Magnin IE, Hoyos MH, Leyton EJFD, Lozano F, Orkisz M. Automatic detection of abnormal vascular cross-sections based on density level detection and support vector machines. *Int J Comput Ass Rad*. 2011; 6:163–174.

Highlights

- We formulate vessel detection on contrast-enhanced computed tomography angiogram images as a Bayesian tracking problem.
- A new vessel detection method by fusing multiple cues extracted from CT images.
- Use of colon atlas and random forest to prune tracking results and reduce false positives.
- Our proposed method showed a significant increase in the F1 score when compared to the traditional Hessian vesselness method.

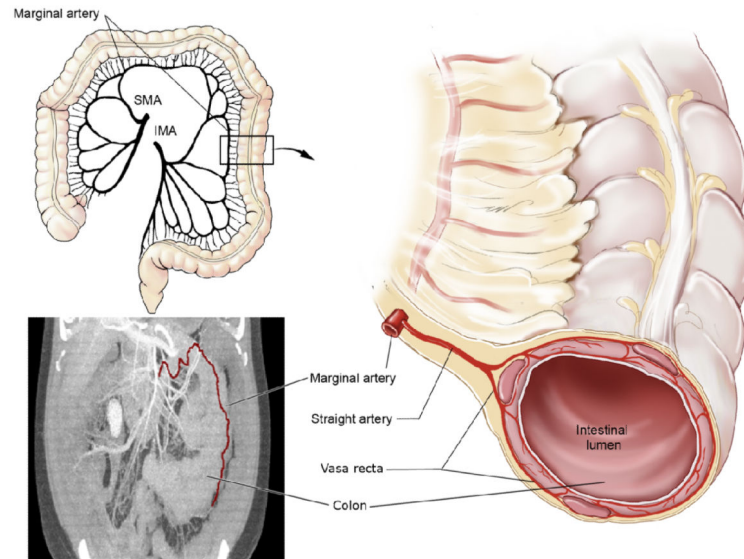


Fig. 1. Illustration of the marginal artery. The marginal artery is an anastomotic channel connecting the superior and inferior mesenteric arteries (SMA and IMA). The marginal artery runs parallel to the colon at a relatively constant distance making this vessel an ideal extrinsic anatomic landmark by which to base a coordinate system of the colon. Segmenting the marginal artery with high fidelity is challenging due to the presence of numerous surrounding straight arteries and vasa recta (bottom left). A ground truth segmentation of the marginal artery is shown in a maximum intensity projection of an abdominal CT examination. [Illustration adapted from (Wei et al., 2013).]

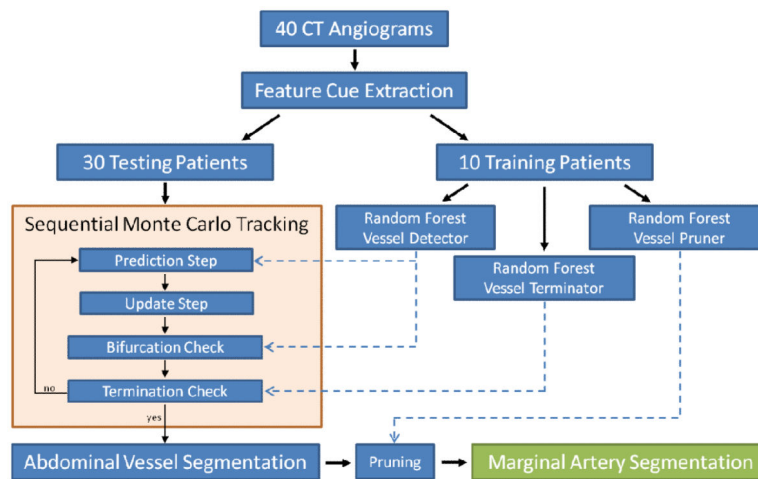


Fig. 2. Workflow for the tracking algorithm. Computed tomography (CT) examinations from 40 patients are randomly split into training and testing sets. All 10 patients in the training set are used to train each of three different random forest classifiers. These classifiers are utilized at different phases of the sequential Monte Carlo (SMC) tracking framework in order to produce the segmented marginal artery. The framework is demonstrated on 30 patients in the testing set. Results from the SMC tracker are fed to a pruning algorithm for false positive reduction.

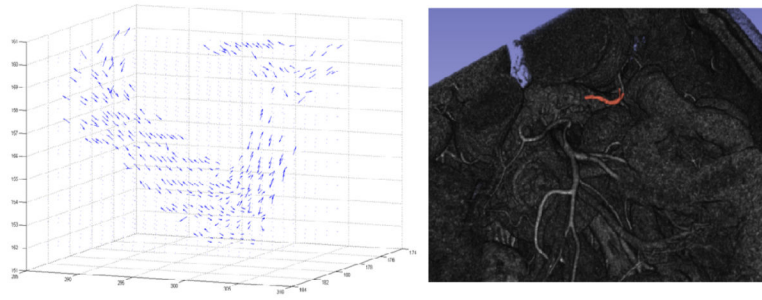


Fig. 3. (Left) 3D eigenvector field plot extracted by Hessian analysis. For eigenvectors (e_1, e_2, e_3) associated with eigenvalues $|\lambda_1| > |\lambda_2| > \lambda_3$, e_3 is the eigenvector associated with the direction of least curvature. Thus, this vector points in the direction of blood flow and can be used to predict vessel movement in tracking. Plot coordinates are in voxel space. (Right) 3D rendering of raw CT volume. The portion of the marginal artery mapped to the vector field on the left is segmented in red. [Left figure reproduced from (Wang, 2013).]

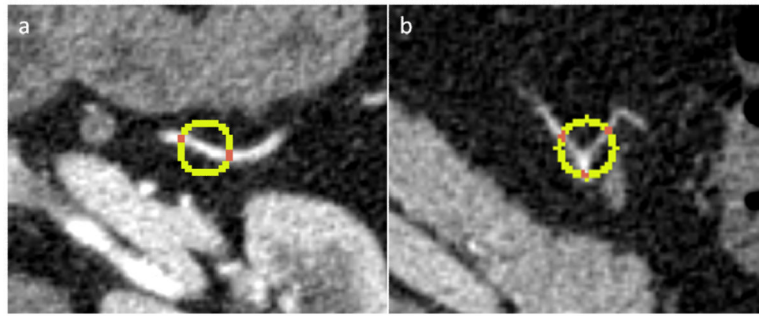


Fig. 4. Example of bifurcation detection using a 3D spherical shell. Images shown are a 2D cross section. The sampling shell centered on the current tracked segment is shown in yellow with high vessel confidence patches in red. a) Two vessel patches were extracted, indicating a straight segment without bifurcation. b) Three patches were extracted, indicating the presence of a bifurcation.

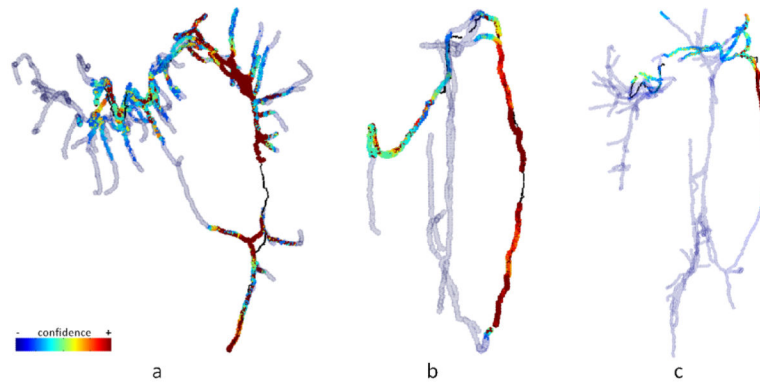


Fig. 5.

3D rendering of the marginal artery pruning algorithm in 3 different patients (a-c, patients 1,2, and 23 from Table S1 respectively). Vessel segmentations from the sequential Monte Carlo (SMC) tracker are pruned to remove false positives using a random forest ensemble learning algorithm. The confidence color scale indicates the confidence assigned to each voxel by the classifier when distinguishing true marginal artery from other abdominal vessels. The dark blue transparent segments were the lowest confidence scores that were easily pruned by thresholding. The ground truth marginal artery centerline is visible in some places as a thin black line. Patient (a) has false positives in the straight arteries, while patients (b) and (c) primarily have false positives in the aorta.

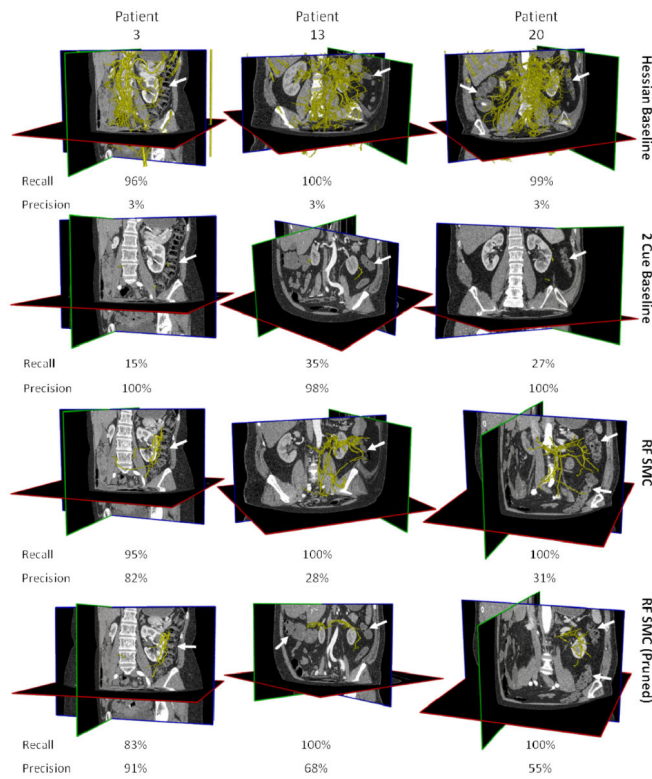


Fig. 6. Marginal artery segmentations (yellow) overlaid on computed tomography (CT) images. The Hessian Baseline is very overgrown and has very low precision. The 2 Cue Baseline tracker terminated after segmenting only a short length of the marginal artery. The random forest-based sequential Monte Carlo (RF SMC) tracker segmented most of the marginal artery along with some false positives. A pruning technique applied to the RF SMC results removed many false positives and improved the precision with only a small decrease in recall. White arrows were added to help point out the colon.

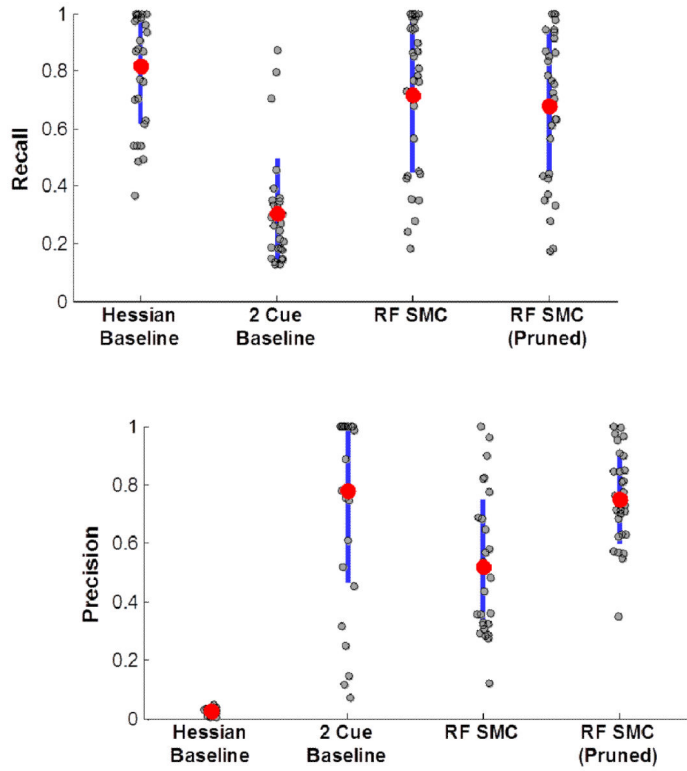


Fig. 7. A comparison of the performance measures for each of the four different methods. Data is shown as mean (red dot) and one standard deviation (blue line) of recall (top) and precision (bottom). Each value for the 30 test patients is shown (gray dots). Horizontal distribution within groups is simply for visualization. Hessian Baseline is the vessel enhancement segmentation and 2 Cue Baseline is a sequential Monte Carlo tracker using two features. These baseline methods are described in Sec. 10.3. The random forest-based sequential Monte Carlo tracking (RF SMC) framework presented in this work is shown without and with the vessel pruning procedure described in Sec. 9.

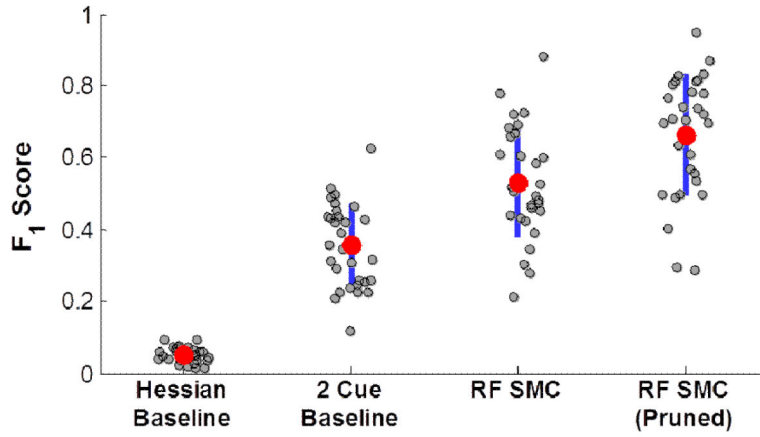


Fig. 8.

A comparison of the performance measures for each of the four different methods. Data is shown as mean (red dot) and one standard deviation (blue line) of the F₁ score. Each value for the 30 test patients is shown (gray dots). Horizontal distribution within groups is simply for visualization. Hessian Baseline is the vessel enhancement segmentation and 2 Cue Baseline is a Monte Carlo tracker using two features. These baseline methods are described in Sec. 10.3. The random forest-based sequential Monte Carlo tracking (RF SMC) framework is shown without and with the vessel pruning procedure described in Sec. 9.

Table 1

Summary of statistical results. ‘*r*’ indicates the recall measures of the pair of methods is statistically significantly different. ‘*p*’ indicates the precision measures of the pair of methods is statistically significantly different. ‘*f*’ indicates the F₁ score of the pair of methods is statistically significantly different. Significance was determined with an overall $\alpha=0.05$ using a paired t-test with a Bonferroni correction to control for familywise errors resulting from multiple comparisons.

	Hessian Baseline	2 Cue Baseline	RF SMC	RF SMC (Pruned)
Hessian	--	<i>r p f</i>	<i>p f</i>	<i>p f</i>
2 Cue Baseline		--	<i>r p f</i>	<i>r f</i>
RF SMC Tracking			--	<i>p f</i>
RF SMC Tracking (Pruned)				--